Plasma Enhanced In Situ Chamber Cleaning Evaluated by Extracted-Plasma-Parameter Analysis

doi: 10.1109/66.492817

Plasma Enhanced *In Situ* Chamber Cleaning Evaluated by Extracted-Plasma-Parameter Analysis

Kazuhide Ino, Iwao Natori, Akihiro Ichikawa, Raymond N. Vrtis, and Tadahiro Ohmi, *Member, IEEE*

Abstract— **We have demonstrated that high-efficiency *in situ* chamber cleaning with short gas residence time is possible for SiO_2 etching chambers by use of NF_3 plasma, and that the end-point determination of the cleaning is possible by monitoring the optical emission intensities of CO or H. Nitrogen trifluoride (NF_3), which has a low N-F bond energy, can generate a plasma with a high density of ions and radicals featuring low kinetic energy. The cleaning efficiency of several halogenated-gas plasmas has been evaluated based on extracted-plasma-parameter analysis. In this analysis important plasma parameters, such as ion energy and ion flux density, can be extracted through a simple rf waveform measurement at the plasma excitation electrode. The accuracy of this technique has been confirmed with a newly developed rf-plasma direct probing method and by ion current measurements.**

I. Introduction

With decreasing device geometry and increasing device performance, the demand for perfect process control becomes ever more important. In the plasma processes such as reactive ion etching (RIE), electron cyclotron resonance (ECR) plasma etching and plasma enhanced chemical vapor deposition (PECVD), the process parameters, however, fluctuate due to plasma sub-product buildup on the chamber walls and internal fixtures and resulting contamination [1], [2]. The parameters are also very susceptible to the chamber inner surface condition [3]–[5]. Therefore it is a necessity to have identical processing chamber conditions at the start of each processing [6]. To this end, the condition of the chamber inner surface must be absolutely clean, or must be stabilized with a pre-deposition layer. The technique of intentionally forming a film on the chamber walls, a pre-deposition layer, guarantees near-identical conditions for subsequent processing; however, such a technique has many problems. The biggest problem is that of particle generation, which is considered one of the major causes of device failures [1]. In order to achieve greater process uniformity and device yield, the establishment of high-efficiency *in situ* chamber cleaning technology is essential.

In the last few decades, a considerable number of studies have been made on dry etching using fluorinated-gas plasmas. Typically, CF_4 [7]–[11], C_2F_6 [9], [10] and SF_6 [11], [12] plasmas have been studied for the etching of Si, SiO_2 and other materials, and have been used for *in situ* chamber cleaning in the microelectronics industry. In some cases, the addition of oxygen into these fluorinated-gases has been performed to maximize the density of the fluorine atoms and, hence, the etch rate. The plasma chemistry and the fundamental properties of an NF_3 etchant gas discharge have been also studied by many researches [13]–[18] and, in some cases, NF_3 plasma has been used for PECVD chamber cleaning [19]. Despite this, little article has been published on cleaning characteristics of NF_3 plasma and its use especially for *in situ* cleaning of etching chambers.

Therefore, the purpose of this paper is to present high-efficiency *in situ* chamber inner surface cleaning technology using NF_3 plasma that will allow for each process to be carried out under identical conditions. According to our experimental results, NF_3 is the best choice for *in situ* chamber cleaning due to its higher ion and radical densities and, hence, superior cleaning characteristics compared to another halogenated-gases, though somewhat expensive and toxic. In this paper, first we describe a convenient plasma-evaluation method, which is called extracted-plasma-parameter analysis [20]–[23], for evaluating the cleaning efficiency of various halogenated specialty gases. This method has enabled us to monitor *in situ* the two important plasma parameters, ion energy and ion flux density, through very simple rf waveform measurements at the powered electrode without introducing any contamination or external disturbances to the discharge. Based on the results of this analysis, high ion and radical density as well as low ion-bombardment energy plasma can be realized. The accuracy of this analysis has been confirmed by a newly developed rf-plasma direct probing method [24], [25] as well as ion current measurements. We also demonstrate that *in situ* chamber cleaning under a high gas flow rate and a high pumping speed enhance the removal of sub-products adhering to the inner surface of SiO_2 etching chambers, and that the end-point determination of the cleaning is possible by monitoring the optical emission intensities of CO or H.

II. Experimental

A. Experimental Setup

The apparatus used in these experiments, which has been described previously [20], is a parallel-plate capacitively coupled RIE equipment with an excitation frequency of 13.56 MHz. The interelectrode distance is 3 cm. The design of this RIE system is based on the Ultra Clean Technology concept [26]–[29]. The electrodes and the chamber are made of stainless steel with mirror-polished surfaces to minimize

The authors are with the Department of Electronic Engineering, Tohoku University, Sendai 980-77, Japan.

K. Ino, I. Natori, and A. Ichikawa are also with the Laboratory for Electronic Intelligent Systems, Research Institute of Electrical Communication, Tohoku University, Sendai 980-77, Japan.

Publisher Item Identifier S 0894-6507(96)03263-0.

outgassing and are covered with quartz fixtures to suppress metallic contamination due to physical sputtering.

Optical emission spectroscopy (OES) (IMUC-7000 spectrometer) with argon as an actinometer was used to measure the relative atomic fluorine concentration [30]. The resolution of the system is 0.15 nm. The emission lines studied are 750.4 nm and 703.7 nm for Ar and F, respectively. The spectral range covered is 195 nm large and allows the simultaneous following of the Ar and F emission lines. Optical emission spectra were also used to evaluate the chamber inner surface condition.

B. Extracted Plasma Parameter Analysis

Several plasma parameters were extracted from the voltage waveform of the powered electrode in order to estimate the electrical characteristics of rf-generated discharges, especially that of positive ions, since the cation has the most important role in plasma processing [31]–[34]. The theoretical background of the analysis has been discussed in detail previously [20], so only a cursory description related to the extraction of the parameters will be given here.

The rf waveforms appearing at the plasma excitation electrode were observed by an oscilloscope using a high voltage probe (Tektronix P6015). The probe was attached directly to the back of the electrode in order to minimize stray impedance effects. The instantaneous voltage of the plasma excitation electrode is expressed by

$$V_{\mathrm{rf}}(t) = V_{\mathrm{rf}o}\sin(\omega t) + V_{\mathrm{dc}}, \quad (V_{\mathrm{dc}} < 0) \tag{1}$$

where $V_{\mathrm{rf}o}$ is the amplitude of the rf waveform, ω is the angular rf driving frequency, and V_{dc} is the self-bias voltage of the powered electrode. The time-averaged plasma potential V_p was estimated using the well known equation [35], [36] in these experiments,

$$V_p = \frac{V_{\mathrm{rf}o} + V_{\mathrm{dc}}}{2}, \quad (V_{\mathrm{dc}} < 0). \tag{2}$$

The ion energy (E_{ion}) bombarding the substrate surface can be defined as the difference between the time-averaged plasma potential and the self-bias voltage of the substrate electrode

$$E_{\mathrm{ion}} = q(V_p - V_{\mathrm{dc}}) \quad (V_{\mathrm{dc}} < 0) \tag{3}$$

where q is the charge of an electron. In addition a new parameter called *ion flux parameter* is introduced as a measure of ion flux density incident on the substrate surface

$$\text{Ion Flux Parameter} = \frac{P}{V_{\mathrm{pp}}} \tag{4}$$

where P is the rf power delivered by power supply and $V_{\mathrm{pp}} = 2V_{\mathrm{rf}o}$. Since P/V_{pp} has the dimensions of current and is related to the plasma density, the parameter can be taken to be a measure of ion flux density [22], [37].

By using these extracted-plasma-parameters, we compare the electrical characteristics and the cleaning efficiency of various halogenated-gas plasmas in Sections III.A and B, respectively.

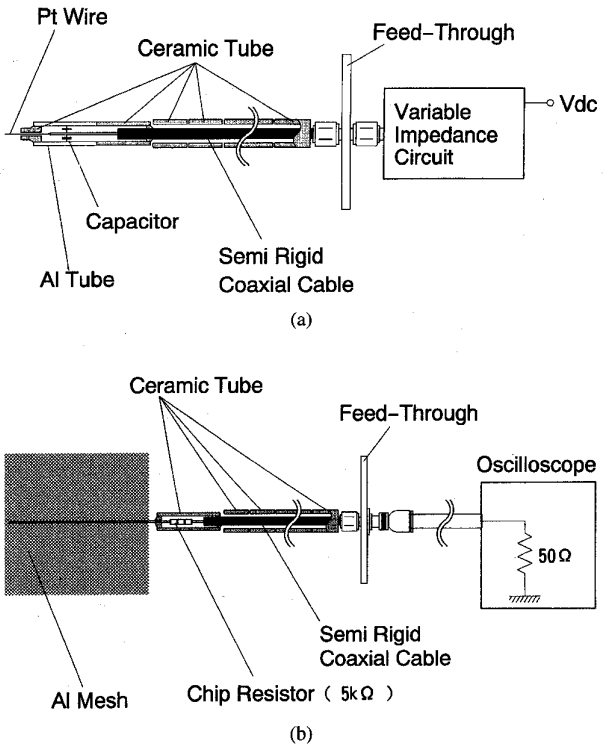

Fig. 1. Schematic diagrams of the advanced Langmuir probe used to measure the time-averaged plasma potential (a), and the newly developed probe used to measure the instantaneous plasma potential (b).

C. Probe Measurements

In order to confirm the accuracy of the plasma potential estimated by use of (2), the rf plasma potential has been directly measured by a newly developed rf-plasma probing method [24], [25]. In this method we have used two types of probes. One is an advanced Langmuir probe that is used to measure the time-averaged plasma potential V_p, as shown in Fig. 1(a). The other is a newly developed probe used to measure the instantaneous plasma potential $V_p(t)$, shown in Fig. 1(b). Here the instantaneous plasma potential means the rf component of the plasma potential. The probes were located centrally within the discharge, with their tips parallel to the electrode surfaces. Normally, probe measurements in rf discharges have severe problems with rf interference [38], [39]. These problems, which are caused by the fluctuating voltage across the probe-plasma sheath, induce a large distortion in the probe characteristics. In order to suppress this type of problems, the rf voltage across the sheath must be minimized by ensuring that the impedance of the sheath is small compared to the impedance between the probe and ground [40]. Therefore, the newly developed probes are designed based upon two fundamental concepts for forcing the probe potential to follow the instantaneous plasma potential. One is increasing the probe-plasma sheath capacitance in order to decrease the sheath impedance, and the other is increasing the impedance between the probe and ground.

The advanced Langmuir probe illustrated in Fig. 1(a) has a 0.5 mm diameter platinum wire as the probe tip. In order to increase the sheath capacitance, an aluminum tube is connected

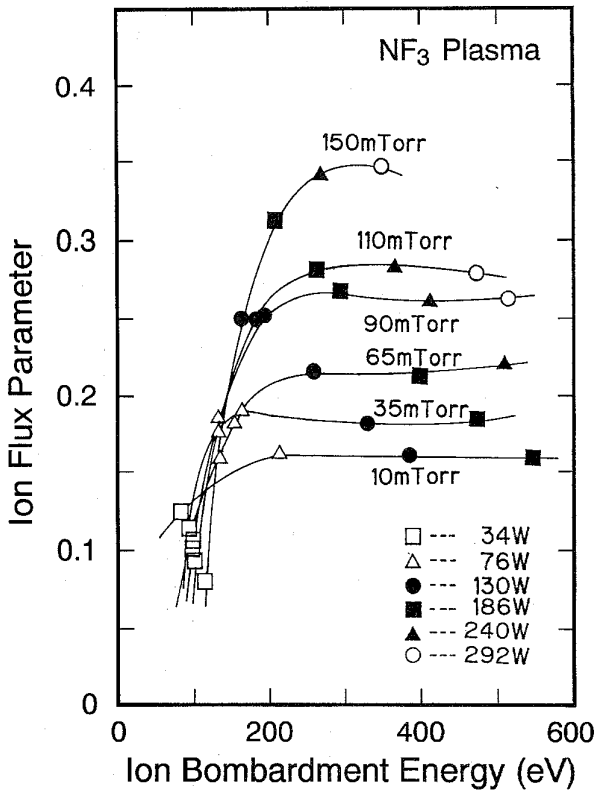

Fig. 2. Relationship between the extracted plasma parameters ($E_{\rm ion}$, ion flux parameter) and the externally adjustable parameters (rf power, gas pressure) for NF_3 plasma.

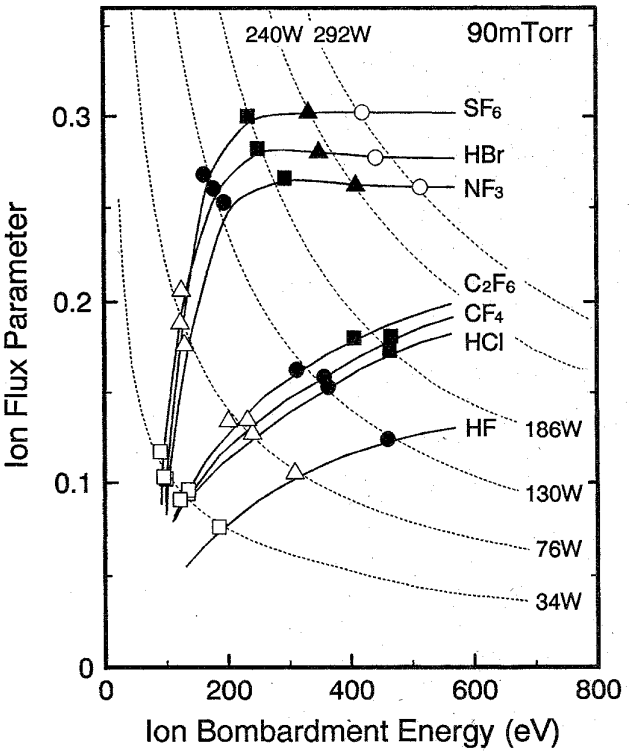

Fig. 3. Relationship between the extracted plasma parameters ($E_{\rm ion}$, ion flux parameter) and rf power for various halogenated-gas plasma at 90 mTorr.

to the wire via a 1000 pF capacitor. Moreover, the impedance between the probe and ground can be maximized by adjusting the variable impedance circuit, which is a parallel LC circuit. Therefore, the rf voltage across the sheath can be minimized by use of this probe, and it yields undistorted characteristics.

The newly developed probe used to measure the instantaneous plasma potential is illustrated in Fig. 1(b). This probe has an aluminum mesh (3 cm × 3 cm) in order to increase the sheath capacitance. Chip-resistors (1 kΩ × 5), which have no dependence on frequency below 100 MHz, are connected between the mesh and the probe body in order to increase the probe impedance, as shown in Fig. 1(b). The probe body is formed by a semi rigid coaxial cable with characteristic impedance of 50 Ω. The cable is connected to an oscilloscope, whose input impedance is adjusted to 50 Ω. Therefore the probe tip (i.e., the aluminum mesh) automatically follows the instantaneous plasma potential, and the waveform of the plasma potential can be observed on the oscilloscope. As a result, this probe acts as a passive voltage-probe with a signal attenuation of 101x.

III. Results and Discussion

A. Plasma Characteristics of Halogenated-Gases

Fig. 2 shows the relationship between the extracted plasma parameters ($E_{\rm ion}$, Flux Parameter) and the externally adjustable parameters (rf power, gas pressure) for an NF_3 plasma. The plasma parameters were extracted from the voltage waveform of the powered electrode by use of (3) and (4). By examining this figure we can get a better understanding of the behavior of ion energy and flux density in an NF_3 plasma. In addition, if the parameters such as the etch rate of subproducts representing the cleaning efficiency are plotted on this figure, they will greatly aid in understanding the cleaning process. These parameters, ion energy and flux density, are more physically meaningful than rf powers or gas pressures. The results of this analysis are discussed in Section III.B.

Fig. 3 compares the relationship between the extracted-plasma-parameters and rf power for various halogenated-gas plasmas at 90 mTorr. From these plasma characteristics, the halogenated-gases can be roughly classified into two groups [23]: One group is consist of C_2F_6, CF_4, HCl, and HF gases, and the other is consist of SF_6, HBr, and NF_3 gases. In the first group, both ion flux and energy increases as rf power increases. In these plasmas, rf power is dissipated by both generation and acceleration of ions. On the other hand, the behavior of ion flux and energy is different in the second group. As rf power increases from 34 W to 130 W, only ion flux density increases while there is little effect on ion bombardment energy. As rf power more increases from 186 W to 292 W, conversely, only ion energy increases while the flux density remains almost constant.

Table I indicates molecular structure, bond distance and mean bond energy of various gas molecules [41]. The mean bond energies of C_2F_6, CF_4, HCl, and HF, which belong to the first group, are larger than those of SF_6, HBr, and NF_3, which belong to the second group. From these results, it is speculated that the plasma characteristics are strongly

TABLE I
MOLECULAR STRUCTURE, BOND DISTANCE AND MEAN BOND ENERGY OF VARIOUS GAS MOLECULES [41]

Molecular Structure	Molecule	Bond Distance (Å)	Mean Bond Energy (eV/molecule)
	N_2	N–N: 1.087	9.76
	O_2	O–O: 1.207	5.12
	H_2	H–H: 0.741	4.48
	Cl_2	Cl–Cl: 1.986	2.48
	HF	H–F: 0.917	5.87
	HCl	H–Cl: 1.274	4.43
	HBr	H–Br: 1.414	3.76
	NF_3	N–F: 1.371	2.83
	SiF_4	Si–F: 1.553	6.14
	CF_4	C–F: 1.323	5.02
	$SiCl_4$	Si–Cl: 2.019	4.11
	CCl_4	C–Cl: 1.767	3.35
	SF_6	S–F: 1.561	3.34
	C_2F_6	C–C: 1.545 C–F: 1.326	4.87

depend on bond energies of gas molecules. The relationship between the plasma parameters and bond energy of various halogenated-gases are discussed in detail in Section III.B.

B. In Situ Chamber Cleaning

First we will describe how dramatic changes in plasma characteristics can occur when sub-products are deposited on a chamber inner surface. Fig. 4 shows the optical emission spectra of an Ar discharges at Fig. 4(a) an initial condition, where the chamber inner surface was completely cleaned by a wet cleaning, and Fig. 4(b) after SiO_2 etching using a CF_4/H_2 plasma for 90 min. When the chamber is clean, only Ar peaks are observed as is seen in Fig. 4(a). However, after SiO_2 etching, SiF and SiF_2 peaks are observed as shown in Fig. 4(b). Peaks corresponding to CO, CO^+, and CO_2^+ are also observed after SiO_2 etching, although the intensity of those are small compared to that of SiF or SiF_2. These peaks appear to originate from the sub-products adhering to the chamber inner surfaces. This is known because analysis of the sub-products using X-ray Photoelectron Spectroscopy (XPS) shows their composition to be mostly carbon, fluorine, oxygen and silicon with some other minor components. These results suggest that the condition of the chamber inner surface can strongly affect that of the discharges. Therefore it is necessary to have identical processing chamber conditions at the start of every process in order to realize fluctuation-free processing.

Next we have evaluated the etch rate of a mixture of photoresist TSMR8900 (Tokyo Ohka Kogyo Co., Ltd.) and an OCD silica solution (Tokyo Okha Kogyo Co., Ltd.), which were spin-coated onto a silicon wafer and then postbaked at

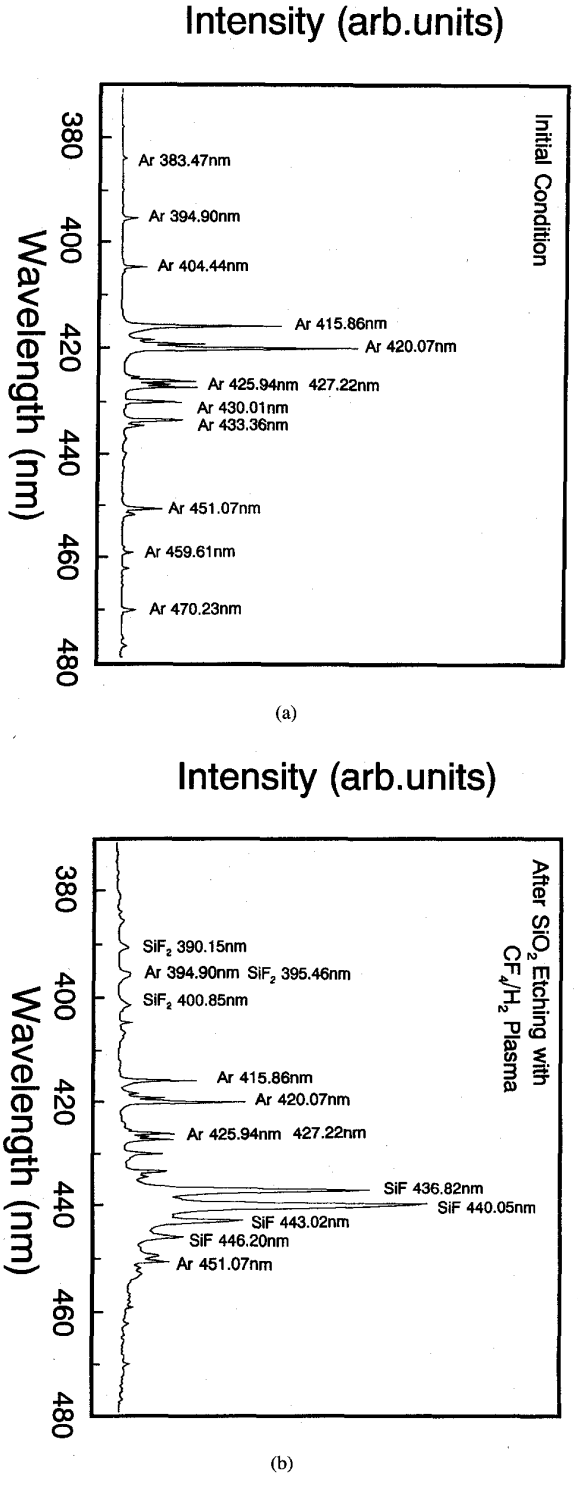

Fig. 4. Optical emission spectra of Ar discharges at initial condition (a), and after SiO_2 etching (b).

130°C. We chose to look at these films in order to model the sub-products found in SiO_2 etching chambers which are notorious for severe particle generation [1]. Fig. 5 shows the etch rate of the simulated sub-products using NF_3, SF_6 C_2F_6, and CF_4 plasmas as a function of bombarding ion energy and

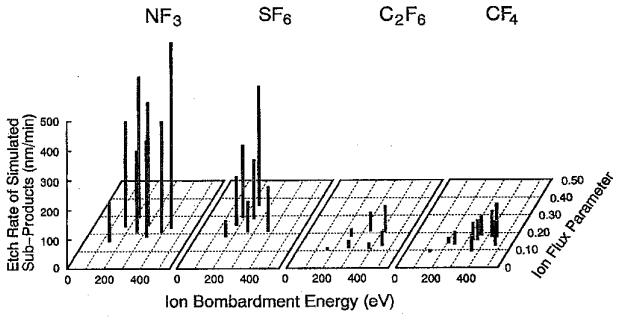

Fig. 5. Etch rate of a mixture of photo resist and silica solution modeling sub-products of SiO_2 etching chambers as a function of ion energy and flux density for NF_3, SF_6, C_2F_6, and CF_4 plasmas.

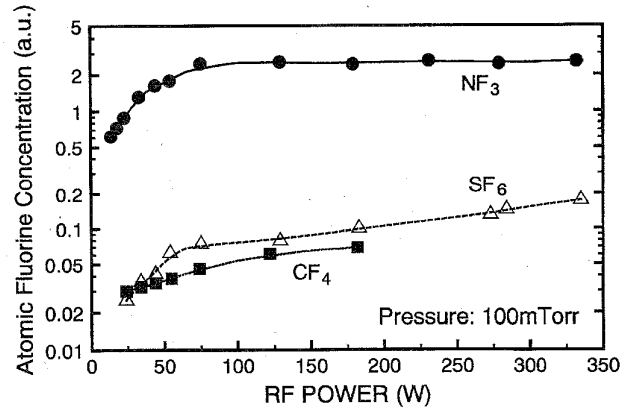

Fig. 6. Atomic fluorine concentration versus rf power for NF_3, SF_6, and CF_4plasmas at 100 mTorr.

ion flux density. In these experiments, the gas flow rate was maintained at 50 sccm. From this figure it can be clearly seen that the cleaning efficiency of the NF_3 discharge is the greatest among these fluorinated gases. In these experiments the sample wafer was located directly on the powered electrode. This means that the sample experienced higher ion bombardment energy than what would be experienced at the chamber walls. However, we hope that similar trends can be extrapolated to the situation at the chamber walls. Thus we can evaluate the cleaning efficiency of various specialty gases using these type of graphs.

Fig. 6 shows the atomic fluorine concentration in a 100 mTorr discharge as a function of rf power for three different fluorinated gases as measured by actinometry [30]. From this figure we can see that the atomic fluorine concentration observed in an NF_3 plasma is at least one order of magnitude higher than that observed in CF_4 or SF_6 plasmas. This is one of the reasons why the etch rate is so much higher for NF_3. This figure also suggests that the discharge is much more effective at dissociating the NF_3 than the CF_4 or SF_6, presumably due to the lower bond energy of the NF_3 molecule as indicated in Table II [13], [42], [43]. Of course, electron-induced dissociation is related to the cross section for excitation to a dissociative state for which the threshold is not just the bond energy for the process. However, we hope to discuss the dissociation of various gases by using the bond energy as one measure [14], [23].

TABLE II
BOND DISSOCIATION ENERGY OF VARIOUS DISSOCIATIVE REACTIONS IN NF_3, SF_6 AND CF_4 DISCHARGES

Reaction	Bond Dissociation Energy [eV/molecule]	Reference
$NF_3 + e \rightarrow NF_2 + F + e$	2.6	13
$NF_2 + e \rightarrow NF + F + e$	2.5	13
$NF + e \rightarrow N + F + e$	3.6	42
$SF_6 + e \rightarrow SF_5 + F + e$	4.0	43
$SF_5 + e \rightarrow SF_4 + F + e$	2.3	43
$SF_4 + e \rightarrow SF_3 + F + e$	3.7	43
$SF_3 + e \rightarrow SF_2 + F + e$	2.7	43
$SF_2 + e \rightarrow SF + F + e$	4.0	43
$SF + e \rightarrow S + F + e$	3.6	42
$CF_4 + e \rightarrow CF_3 + F + e$	5.6	13
$CF_3 + e \rightarrow CF_2 + F + e$	3.8	13
$CF_2 + e \rightarrow CF + F + e$	5.4	13
$CF + e \rightarrow C + F + e$	5.7	42

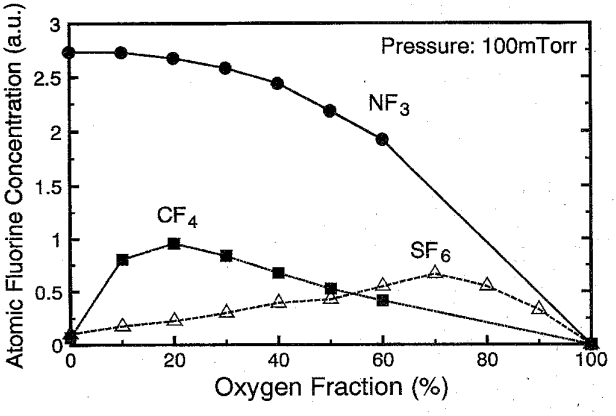

Fig. 7. Atomic fluorine concentration versus percent oxygen for NF_3, SF_6, and CF_4 gas mixture plasmas at 100 mTorr pressure and 180 W rf power.

Fig. 7 shows the effect of adding oxygen into NF_3, SF_6 and CF_4 discharges on the atomic fluorine concentration. The gas pressure and rf power were maintained at 100 mTorr and 180 W, respectively. This figure indicates that although the atomic fluorine concentration in CF_4 discharge increases as up to 20% oxygen is added, the atomic fluorine concentration is still two times lower than that seen in NF_3 discharges. We can also see from Fig. 7 that there is some slight chemical interaction between SF_6 and oxygen which causes an increase in the atomic fluorine concentration at high levels of oxygen. From these results it has been confirmed that NF_3 is the most suitable gas for *in situ* chamber cleaning among these fluorinated gases. The NF_3 plasma is also advantageous because the possibility of re-deposition of side-products is lower. By contrast, CF_4 C_2F_6 or SF_6 discharges are often undesirable because of the carbonaceous or sulfurous chamber inner surface contamination.

Fig. 8 shows the relationship between the mean bond energy and plasma parameters for several fluorinated gases (Fig. 8(a)) and halogenated gases (Fig. 8(b)). The filled triangles (▲)

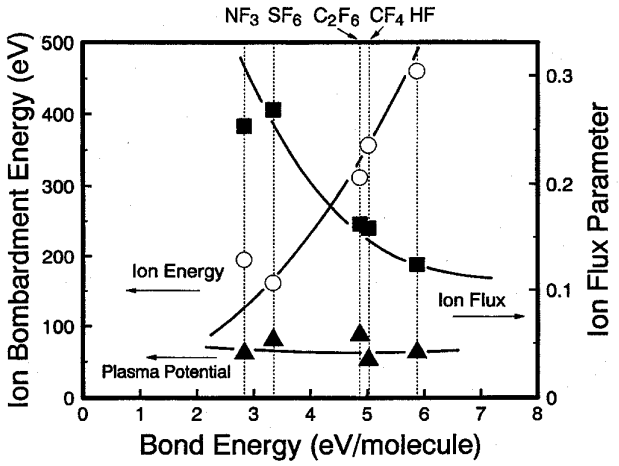

(a)

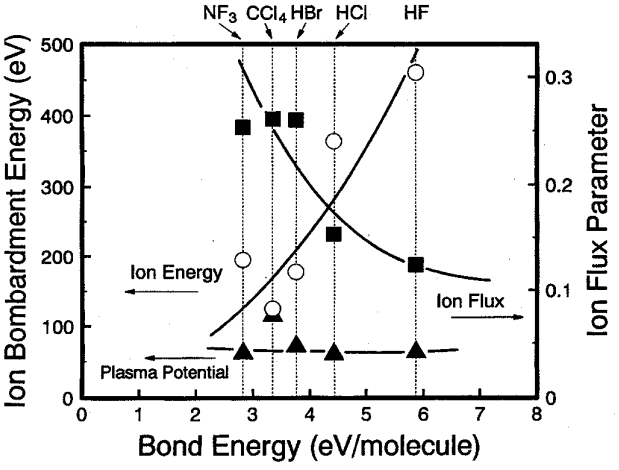

(b)

Fig. 8. Relationship between the mean bond energy and estimated plasma parameters, such as ion bombardment energy (○), ion flux parameter (■) and the time-averaged plasma potential (▲) for several fluorinated gas plasmas (a), and halogenated gas plasmas (b).

indicate the time-averaged plasma potential, the open circles (○) indicate ion bombardment energy and the filled squares (■) indicate the ion flux parameter. The pressure and rf power were maintained at 90 mTorr and 130 W, respectively, in these experiments. These plasma parameters were extracted from the voltage waveform of the powered electrode by use of (2)–(4). It is interesting to see that these plasma parameters seem to depend on the mean bond energy. As the bond energy decreases, the ion bombardment energy also decreases. On the contrary, the ion flux density increases with decreasing the bond energy. However, the time-averaged plasma potential dose not appear to be strongly depend on the bond energy. These results lead to the conclusion that the optimal gases for *in situ* chamber cleaning are halogenated gases with low bond energy such as NF_3, CCl_4, and HBr that can generate a high density of ions as well as radical species in the plasma.

Next we examined the cleaning efficiency of NF_3, CCl_4, and HBr plasmas as is shown in Fig. 9. It can been seen from

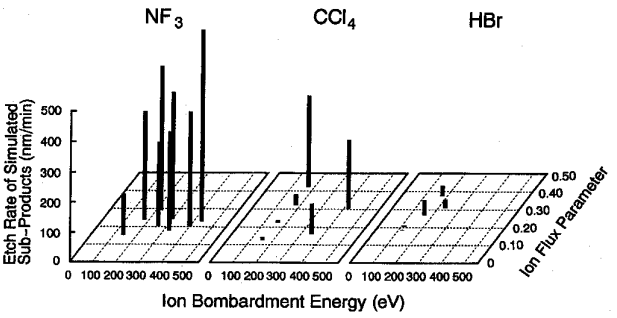

Fig. 9. Etch rate of simulated sub-products of SiO_2 etching chambers as a function of ion energy and flux density for NF_3, CCL_4, and HBr plasmas.

TABLE III
BOND ENERGY OF SEVERAL HALOGENATED SILICON IN A DIATOMIC MOLECULE [42]

	Bond Energy [eV/molecule]
Si-F	5.7
Si-Cl	4.2
Si-Br	3.8

these graphs that the etch rate of simulated sub-products is the greatest when fluorinated gas is used, while chlorinated gas and brominated gas provide only slow etching. When the sub-products are etched by the halogenated gases, one of the main reaction-products would be halogenated silicon, Si–X (X; halogen). Table III indicates a list of the chemical bond strength of halogenated silicon in a diatomic molecule [42]. The higher the chemical bond strength is, the more easily diatomic molecules are formed. Si–F exhibits a higher bond energy than Si–Cl or Si–Br. Thus NF_3 plasma could achieve higher etch rate than CCl_4 or HBr plasma. Based on these results, NF_3 is the best choice for *in situ* chamber cleaning.

Fig. 10 shows the etch rate of the simulated sub-products as a function of the NF_3 gas residence time τ, which is calculated using the following equation [44].

$$\tau = \frac{V}{S} = \frac{pV}{pS} = \frac{pV}{Q}. \tag{5}$$

Here, V is the chamber volume, S is the pumping speed, p is the gas pressure, and Q is the gas flow rate. The gas pressure and the rf power for these experiments were maintained at 10 mTorr and 150 W, respectively, thus the ion bombardment energy was fixed at 320 eV. Reduction in the gas residence time resulted in a dramatic increase in the etch rate. The reason for the increased etch rate is that the reduction in the gas residence time causes the effective evacuation of reaction products, and that the increase in the flow rate provides sufficient active etching spices [45]–[48]. It is also expected that the effective evacuation will suppress sub-products re-deposition onto chamber walls and internal fixtures. Therefore it is confirmed that *in situ* chamber cleaning with a high gas flow rate and a high pumping rate can enhance the removal of the sub-products adhering to chamber walls and internal fixtures. However, the flow rate of the cleaning gas must be optimized in order to realize both the sufficient etch rate and the minimum gas consumption.

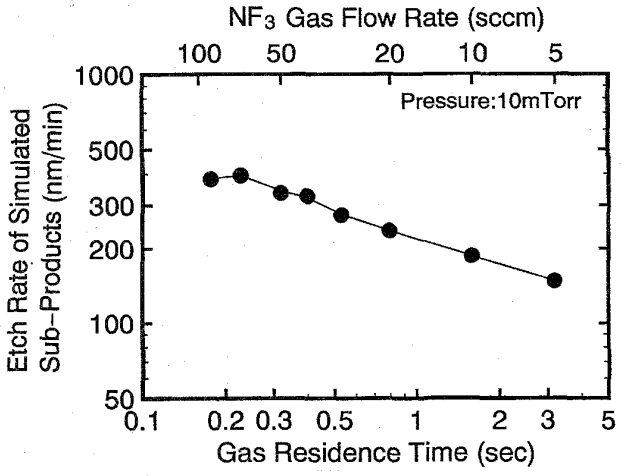

Fig. 10. Etch rate of simulated sub-products of SiO_2 etching chambers as a function of gas residence time for NF_3 plasma at a constant pressure of 10 mTorr.

Fig. 11(a) shows a photograph of a grounded electrode after SiO_2 etching using CF_4/H_2 plasma for 10 h, where the total pressure was 45 mTorr and the flow rates of CF_4 and H_2 were 15 and 10 sccm, respectively. The grounded electrode appears brown due to adhered sub-products. Fig. 11(b) shows the same electrode after *in situ* chamber cleaning with NF_3 plasma for 30 min. It can be clearly seen from this photograph that the sub-products have been completely removed from the electrode. The cleaning conditions were rf power of 300 W, NF_3 gas flow rate of 50 sccm, and a pressure of 100 mTorr. This again confirms that high-efficiency *in situ* chamber cleaning is possible for SiO_2 RIE chambers by using NF_3 plasma.

Fig. 12 shows the optical emission spectra of Ar discharges at various chamber inner surface conditions, where the gas pressure and rf power were maintained at 100 mTorr and 150 W, respectively. The spectra shown in Fig. 12(a) and (b) are the same as those shown in Fig. 4(a) and (b), respectively. Fig. 12(c) shows the optical emission spectrum of Ar discharge, which was measured after *in situ* chamber cleaning with NF_3 plasma for 15 min. Even after the plasma cleaning SiF and SiF_2 peaks are observed. The peak intensity, however, decreases. These peaks are thought to originate from the residual fluorine adsorbed onto the quartz fixtures because the sub-products are completely removed by the cleaning as demonstrated in Fig. 11. During *in situ* chamber cleaning with NF_3 plasma, the emission intensities of CO and H were measured as a function of time. Fig. 13 shows the variation in the CO and H peaks during the NF_3 plasma cleaning, where the measured emission lines are 483.5 nm and 486.1 nm for CO and H, respectively. Fig. 14 shows the optical emission spectra of the NF_3 plasma measured at 1 min 30 s (a) and 10 min (b) after the discharge was struck. These results suggest that the sub-products were removed by the cleaning after about 5 min, and that the OES measurement of the CO or H emission lines makes it possible to determine an end-point of the *in situ* chamber cleaning. Thus it is reasonable to suggest that the SiF and SiF_2 peaks shown in Fig. 12(c) are originated from

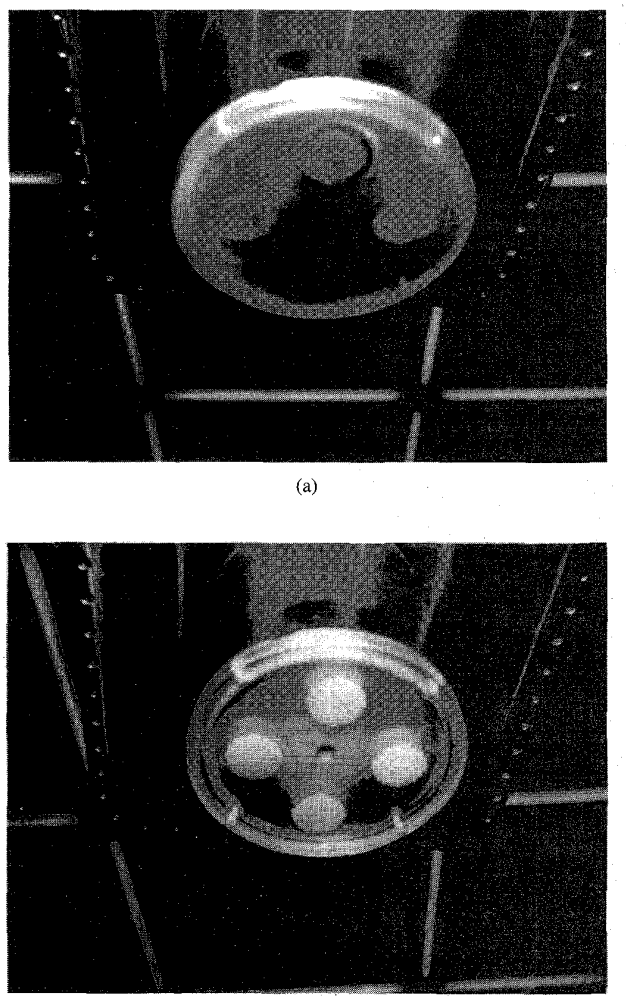

(a)

(b)

Fig. 11. Photographs of the grounded electrode after SiO_2 etching for 10 h (a), and after *in situ* chamber cleaning with NF_3 plasma for 30 min (b).

the residual fluorine adsorbing onto the quartz fixtures and not from the sub-products. Following the NF_3 plasma cleaning, an Ar/H_2 plasma cleaning was performed for 10 min, which is a highly reducing ambient. The gas flow rates of Ar and H_2 were 50 and 25 sccm, respectively, the total gas pressure was 100 mTorr and the rf power was 150 W. Fig. 12(d) shows the spectrum of Ar discharge measured after the Ar/H_2 plasma cleaning. The spectrum is almost identical with the initial one shown in Fig. 12(a). Therefore, *in situ* chamber cleaning is possible for SiO_2 etching chambers by use of a NF_3 plasma cleaning followed by a Ar/H_2 plasma cleaning. This cleaning technique would also be applicable for etching, sputtering and PECVD chambers for silicon or silicon compounds.

C. Plasma Parameter Measurement

In order to verify the accuracy of extracted-plasma-parameters such as the time-averaged plasma potential, ion energy and ion flux parameter, the electrical characteristics of rf discharges have been precisely measured. Fig. 15 shows the waveforms of the plasma potential $V_p(t)$ and the powered

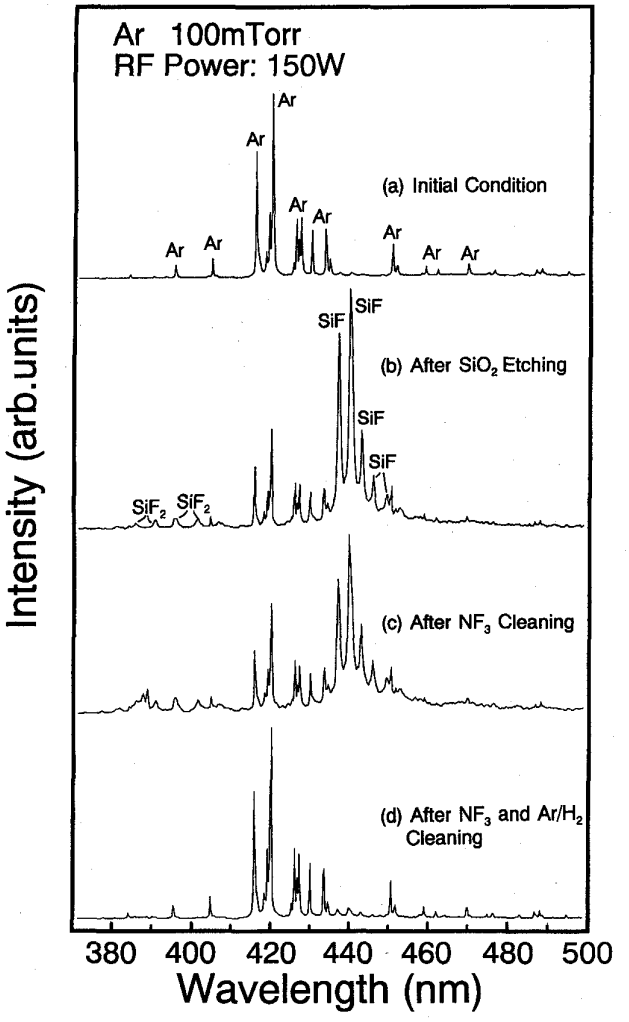

Fig. 12. Optical emission spectra of Ar discharges at initial condition (a), after SiO_2 etching for 90 min (b), after NF_3 plasma cleaning for 15 min (c), and after Ar/H_2 plasma cleaning for 10min (d).

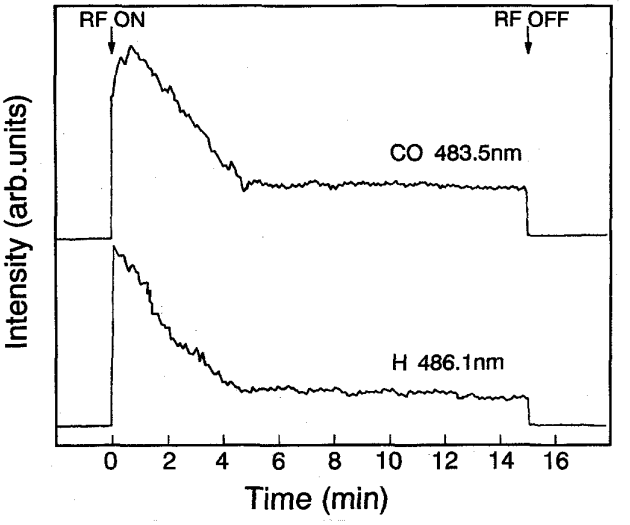

Fig. 13. Optical emission intensities of CO (483.5 nm) and H (486.1 nm) as a function of time during NF_3 plasma cleaning.

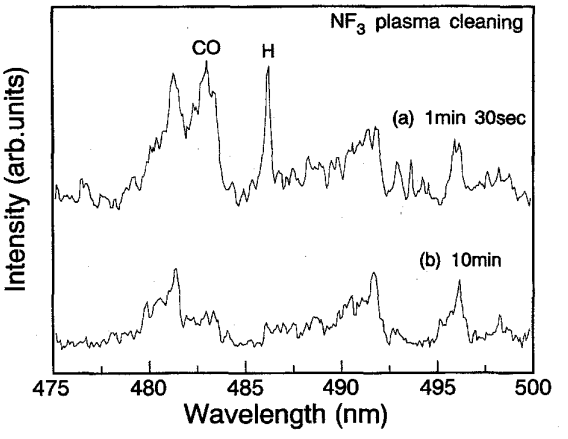

Fig. 14. Optical emission spectra at 1 min 30 s (a) and 10 min (b) during NF_3 plasma cleaning.

electrode voltage $\bar{V}_{\rm rf}(t)$ at 60 mTorr in an Ar discharge, where the rf input power is 15 W. By use of the two newly developed probes illustrated in Fig. 1, the plasma potential has been measured accurately. The dc component of the plasma potential, which represents the time-averaged plasma potential, was measured by the advanced Langmuir probe illustrated in Fig. 1(a). The rf component of the plasma potential, which represents the instantaneous plasma potential, was measured by the newly developed mesh probe and an oscilloscope as shown in Fig. 1(b). Using these two probes and a high-voltage probe connected to the powered electrode, the relationship between the plasma potential and the rf electrode voltage has been clarified. The important point to note is the distortion of the plasma potential and the phase shift between the plasma potential and the rf electrode voltage. In general, it is thought that the waveform of the plasma potential is sinusoidal and in phase with the rf electrode voltage for the simplified capacitive model of the sheath [36]. Thus a distortion of the measured waveform, namely, the existence of the harmonic components seems to be caused by the increased conductive current (i.e., the positive ion current and the electron current) flowing directly through the sheath [36], [49], [50], which is significant compared to the displacement current for the resistive model of the sheath. The phase shift between the plasma potential and the rf electrode voltage suggests that there are resistive components in the discharge [51] between the grounded electrode and the point where the probe was located. (The probe was located in the middle of two electrodes).

Fig. 16 compares the rf power dependence of the time-averaged plasma potentials obtained by two different methods, here the Ar gas pressure was 60 mTorr. The open squares (□) indicate points measured using the advanced Langmuir probe, while the filled circles (•) indicate points estimated from the voltage waveform of the plasma excitation electrode by use of (2). As can be seen in the graph, values estimated from voltage waveforms are in good agreement with those which are accurately measured by the new Langmuir probe. Therefore it is confirmed that the time-averaged plasma potential can be estimated through a simple rf waveform measurement.

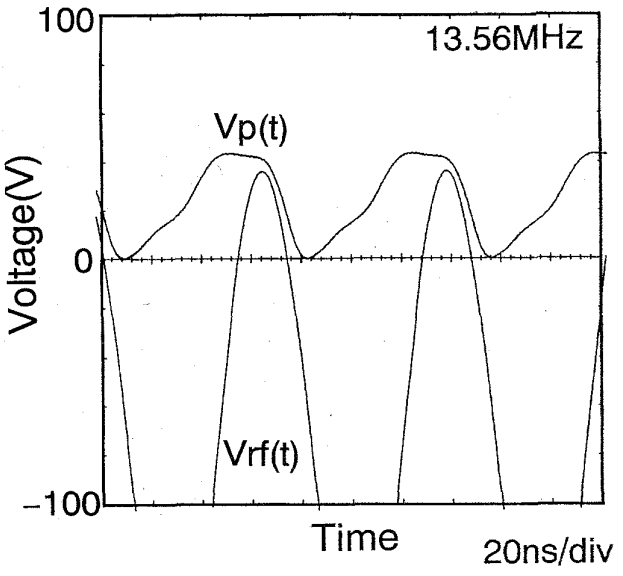

Fig. 15. Waveforms of plasma potential $V_p(t)$ and plasma excitation electrode voltage $V_{\rm rf}(t)$ at 60 mTorr in argon. The rf power is 15 W.

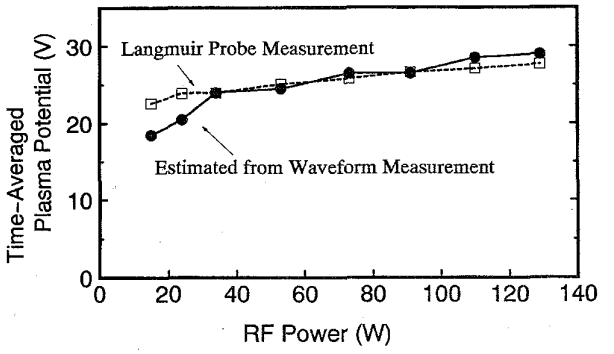

Fig. 16. The rf power dependence of the time-averaged plasma potential-which was measured by the advanced Langmuir probe (□) and estimated from the voltage waveform of the plasma excitation electrode by use of (2) (•).

Next, in order to discuss the slight difference between the two values shown in Fig. 16, the time-averaged plasma potential V_p measured by the advanced Langmuir probe is re-plotted versus $V_{\rm rfo} + V_{\rm dc}$ in Fig. 17 for 20, 60, and 100 mTorr of Ar. The floating voltage V_f of the Langmuir probe is also plotted in the graph, where the probe impedance was maximized. The dashed line indicates the estimated plasma potential $1/2(V_{\rm rfo} + V_{\rm dc})$ based on (2). When $V_{\rm rfo} + V_{\rm dc}$ is small, (2) is a relatively poor representation of V_p. The reason for this is that the potential difference between the plasma potential and the floating voltage $(V_p - V_f)$ and the phase shift between the instantaneous plasma potential $V_p(t)$ and the rf electrode voltage $\bar{V}_{\rm rf}(t)$ were omitted when (2) was derived for the simplified capacitive model of the sheath [36], however, there is a potential difference and phase shift as indicated in Fig. 15. Also, the potential difference $V_p - V_f$ is almost constant at the same gas pressure. Thus, it becomes significant in comparison with smaller $V_{\rm rfo} + V_{\rm dc}$ at lower-power levels. There are also slight discrepancies

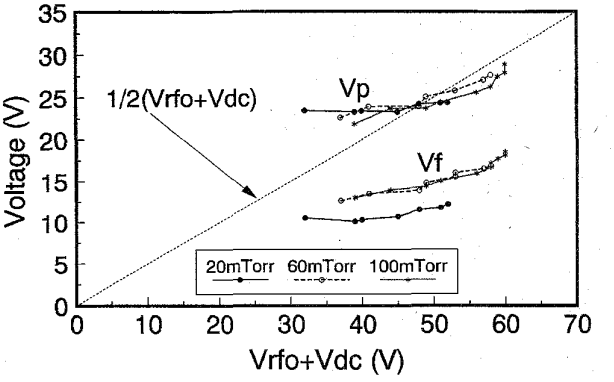

Fig. 17. Time-averaged plasma potential V_p measured by the advancedLangmuir probe is plotted versus $V_{\rm rfo} + V_{\rm dc}$. The floating voltage V_f ofthe Langmuir probe is also plotted. Values obtained from (2) is shown by the dashed line.

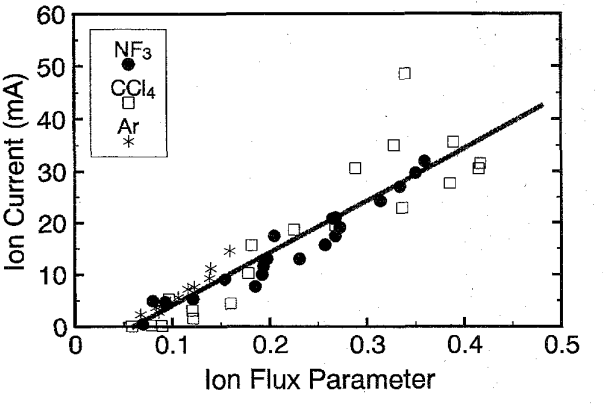

Fig. 18. Relationship between ion flux parameter estimated by use of (4) and the measured ion current.

between the measured plasma potential and the dashed line representing $1/2(V_{\rm rfo} + V_{\rm dc})$ at higher-power levels. This discrepancy would be caused by the increased positive ion current flowing through the sheath. As the conductive current increases in magnitude relative to the displacement current, the waveform of the plasma potential becomes the distorted one [36], [49], [50]. As a result, the time-averaged plasma potential V_p is decreased at higher-power levels. When these slight discrepancies become significant problems, the time-averaged plasma potential should be estimated using the graph shown in Fig. 17. However, in most cases the ion energies are much higher than the discrepancies, therefore, the time-averaged plasma potential and the bombardment energy of ions incident on the substrate surface can be estimated using (2) and (3), respectively.

Fig. 18 shows the relationship between the ion flux parameter calculated using (4) and the ion current fed into the rf electrode for NF_3, CCl_4, and Ar. The ion current was determined by measuring the saturation current while the dc voltage of the electrode was continuously changed to the side of negative bias. The ion current is almost proportional to the flux parameter, therefore, by use of this new parameter we can estimate the ion flux density. However, the straight line drawn in the graph does not pass through the origin. If the flux

parameter indicates the ion flux density, the line would indeed pass through the origin. The precision with which V_{pp} are measured in this work is adequate to eliminate measurement uncertainty as the reason for the nonzero intercept in Fig. 18. The most likely explanation for the failure of the line to pass through the origin is that the rf power measured at the rf generator includes not only the power-loss in the discharge but also that of a matching network and parasitic resistance. The ion flux parameter, however, can be used as a measure of ion flux density. Therefore the accuracy of extracted-plasma-parameter analysis has been confirmed.

IV. Conclusion

We have demonstrated that high-efficiency plasma-enhanced *in situ* chamber cleaning with short gas residence time is possible for SiO_2 etching chambers using NF_3 gas which has a low N–F bond energy, and that the end-point determination of the NF_3 plasma cleaning is possible by monitoring the optical emission intensities of CO or H. If the residual fluorine remaining in the chamber after the cleaning causes severe problems, it can be removed by employing an Ar/H_2 plasma cleaning. The accuracy of extracted-plasma-parameter analysis, which was used to evaluate the cleaning efficiency of various gases, has also been verified by the accurate characterization of rf-generated plasmas using a new probe measurement technique and by ion current measurements. Moreover, the rf-excited plasma potential has been measured directly by the probe method, which has clarified the relationship between the plasma potential and the rf electrode voltage.

Acknowledgment

The authors wish to thank J. Sawahata and M. Hirayama for help with the probe measurements. This study was carried out at the Super Clean Room of Laboratory for Electronic Intelligent Systems, Research Institute of Electrical Communication, Tohoku University.

References

[1] J. Martsching, J. Amthor, and K. Mautz, "Reduction of *in situ* particle formation during contact and via etch processes on downstream oxide etchers," in *Ext. Abstr. 184th ECS Meet.*, New Orleans, 1993, no. 326, p. 536.

[2] M. Nakamura, K. Iizuka, and H. Yano, "Very high selective n^+ poly-Si RIE with carbon elimination," *Jpn. J. Appl. Phys.*, vol. 28, no. 10, pp. 2142–2146, 1989.

[3] A. J. Watts and W. J. Varhue, "Loading effect on quartz microwave window on SF_6 plasma in an electron cyclotron resonance reactor," *Appl. Phys. Lett.*, vol. 61, no. 5, pp. 549–550, 1992.

[4] S. Takahashi, T. Watanabe, S. Miyoshi, A. Ohki, K. Kawada, M. Nakamura, M. S. K. Chen, and T. Ohmi, "Thermal decomposition characteristics of SiH_4," in *ECS Softbound Proc. Series*, PV92-21, D. N. Schmidt, Ed. Pennington, NJ: Electrochemical Society, 1992, pp. 455–477.

[5] T. Ohmi, T. Watanabe, M. S. K. Chen, K. Kawada, A. Ohki, M. Nakamura, and K. Hirao, "Effects of diluent gases and dilution rates on the silane thermal decomposition behaviors on the polysilicon surface," to be published in *J. Electrochem. Soc.*

[6] T. Ohmi, *Breakthrough for Scientific Semiconductor Manufacturing in 2001—A Proposal from Tohoku University, a Special Issue of Break Through*, Realize, Tokyo, no. 71, p. 36, 1992.

[7] C. J. Mogab, A. C. Adams, and D. L. Flamm, "Plasma etching of Si and SiO_2—The effect of oxygen additions to CF_4 plasmas," *J. Appl. Phys.*, vol. 49, no. 7, pp. 3796–3803, 1978.

[8] J. W. Coburn and H. F. Winters, "Plasma etching—A discussion of mechanisms," *J. Vac. Sci. Technol.*, vol. 16, no. 2, pp. 391–403, 1979.

[9] M. J. Kushner, "A kinetic study of the plasma-etching process. I. A model for the etching of Si and SiO_2 in C_nF_m/H_2 and C_nF_m/O_2 plasmas," *J. Appl. Phys.*, vol. 53, no. 4, pp. 2923–2938, 1982.

[10] P. E. Riley, V. D. Kulkarni, and S. H. Bishop, "Examination of fluorocarbon-based plasmas used in the selective and uniform etching of silicon dioxide by response-surface methodology: Effect of helium addition," *J. Vac. Sci. Technol. B*, vol. 7, no. 1, pp. 24–34, 1989.

[11] G. Turban and M. Rapeaux, "Dry etching of polyimide in O_2–CF_4 and O_2–SF_6 plasmas," *J. Electrochem. Soc.*, vol. 130, no. 11, pp. 2231–2236, 1983.

[12] R. d'Agostino and D. L. Flamm, "Plasma etching of Si and SiO_2 in SF_6–O_2 mixtures," *J. Appl. Phys.*, vol. 52, no. 1, pp. 162–167, 1981.

[13] V. M. Donnelly, D. L. Flamm, W. C. Dautremont-Smith, and D. J. Werder, "Anisotropic etching of SiO_2 in low-frequency CF_4/O_2 and NF_3/Ar plasmas," *J. Appl. Phys.*, vol. 55, no. 1, pp. 242–252, 1984.

[14] K. E. Greenberg and J. T. Verdeyen, "Kinetic processes of NF_3 etchant gas discharges," *J. Appl. Phys.*, vol. 57, no. 5, pp. 1596–1601, 1985.

[15] M. Konuma and E. Bauser, "Mass and energy analysis of gaseous species in NF_3 plasma during silicon reactive ion etching," *J. Appl. Phys.*, vol. 74, no. 1, pp. 62–67, 1993.

[16] A. J. Sidhwa, F. C. Goh, H. A. Naseem, and W. D. Brown, "Reactive ion etching of crystalline silicon using NF_3 diluted with H_2," *J. Vac, Sci. Technol. A*, vol. 11, no. 4, pp. 1156–1160, 1993.

[17] K. E. Greenberg, G. A. Hebner, and J. T. Verdeyen, "Negative ion densities in NF_3 discharges," *Appl. Phys. Lett.*, vol. 44, no. 3, pp. 299–300, 1984.

[18] T. Honda and W. W. Brandt, "Mass spectrometric transient study of DC plasma etching of Si in NF_3 and NF_3/O_2 mixtures," *J. Electrochem. Soc.*, vol. 131, no. 11, pp. 2667–2670, 1984.

[19] G. Bruno, P. Capezzuto, G. Cicala, and P. Manodoro, "Study of the NF_3 plasma cleaning of reactors for amorphous silicon deposition," *J. Vac. Sci. Technol. A*, vol. 12, no. 3, pp. 690–698, 1994.

[20] T. Yamashita, S. Hasaka, I. Natori, H. Fukui, and T. Ohmi, "Minimizing damage and contamination in RIE processes by extracted-plasma-parameter analysis," *IEEE Trans. Semicond. Manuf.*, vol. 5, no. 3, pp. 223–233, 1992.

[21] T. Yamashita, S. Hasaka, I. Natori, and T. Ohmi, "Plasma-parameter-extraction for minimizing contamination and damage in RIE processes," *IEICE Trans. Electron.*, vol. E75-C, no. 7, pp. 839–843, 1992.

[22] S. Hasaka, I. Natori, T. Yamashita, and T. Ohmi, "Variation of ion flux in various gas plasmas with 13.56 MHz cathode coupled parallel-plate plasma equipment," in *Ext. Abstr. 181st ECS Meet.*, St. Louis, 1992, no. 66, pp. 107–108.

[23] T. Yamashita, S. Hasaka, I. Natori, H. Fukui, and T. Ohmi, "Extracted-plasma-parameter analysis for minimizing damage and contamination in RIE process," in *ECS Softbound Proc. Series*, V. E. Akins and H. Harada, Eds., PV92-8. Pennington, NJ: Electrochemical Society, 1992, pp. 192–229.

[24] M. Hirayama, W. Shindo, and T. Ohmi, "Impact of high-precision RF-plasma control of very-low-temperature silicon epitaxy," *Jpn. J. Appl. Phys.*, vol. 33, pp. 2272–2275, 1994.

[25] M. Hirayama and T. Ohmi, in preparation for publication.

[26] T. Ohmi, "Ultraclean technology: ULSI proceeding's crucial factor," *Microcontamination*, vol. 6, pp. 49–58, 1988.

[27] ——, "Future trends and applications of ultra clean technology," in *IEDM Tech. Dig.*, Washington, DC, pp. 49–52, 1989.

[28] ——, "ULSI reliability through ultraclean processing," in *Proc. IEEE*, 1993, vol. 81, no. 5, pp. 716–729.

[29] ——, "Scientific semiconductor manufacturing based on ultraclean processing concept," in *Proc. Int. Conf. Advanced Microelectronic Devices and Processing*, Sendai, 1994, pp. 3–22.

[30] J. W. Coburn and M. Chen, "Optical emission spectroscopy of reactive plasmas: A method for correlating emission intensities to reactive particle density," *J. Appl. Phys.*, vol. 51, no. 6, pp. 3134–3136, 1980.

[31] T. Ohmi, T. Ichikawa, H. Iwabuchi, and T. Shibata, "Formation of device-grade epitaxial silicon films at extremely low temperatures by low-energy bias sputtering," *J. Appl. Phys.*, vol. 66, no. 10, pp. 4756–4766, 1989.

[32] T. Ohmi, K. Hashimoto, M. Morita, and T. Shibata, "Study on further reducing the epitaxial silicon temperature down to 250°C in low-energy bias sputtering," *J. Appl. Phys.*, vol. 69, no. 4, pp. 2062–2071, 1991.

[33] T. Ohmi, T. Saito, M. Otsuki, T. Shibata, and T. Nitta, "Formation of copper thin films by a low kinetic energy particle process," *J. Electrochem. Soc.*, vol. 138, no. 4, pp. 1089–1097, 1991.

[34] T. Nitta, T. Ohmi, M. Otsuki, T. Takewaki, and T. Shibata, "Electrical properties of giant-grain copper thin films formed by a low kinetic energy particle properties," *J. Electrochem. Soc.*, vol. 139, no. 3, pp. 922–927, 1992.

[35] J. W. Coburn and E. Kay, "Positive-ion bombardment of substrates in rf diode glow discharge sputtering," *J. Appl. Phys.*, vol. 43, no. 12, pp. 4965–4971, 1972.
[36] K. Köhler, J. W. Coburn, D. E. Horne, E. Kay, and J. H. Keller, "Plasma potentials of 13.56-MHz rf argon glow discharges in a planar system," *J. Appl. Phys.*, vol. 57, no. 1, pp. 59–66, 1985.
[37] R. Petri, D. Henry, and N. Sadeghi, "Tungsten etching mechanisms in low-pressure SF_6 plasma," *J. Appl. Phys.*, vol. 72, no. 7, pp. 2644–2651, 1992.
[38] A. P. Paranjpe, J. P. McVittie, and S. A. Self, "A tuned Langmuir probe for measurements in rf glow discharges," *J. Appl. Phys.*, vol. 67, no. 11, pp. 6718–6727, 1990.
[39] N. St. J. Braithwaite, N. M. P. Benjamin, and J. E. Allen, "An electrostatic probe technique for RF plasma," *J. Phys.*, vol. E-20, pp. 1046–1049, 1987.
[40] R. R. J. Gagne and A. Cantin, "Investigation of an rf plasma with symmetrical and asymmetrical electrostatic probes," *J. Appl. Phys.*, vol. 43, no. 6, pp. 2639–2647, 1972.
[41] Japan Chemical Society, Ed., *Chemical Handbook*, 3rd Ed., Fundamental II, Maruzen, Tokyo, 1984, pp. 322–323, in Japanese.
[42] R. C. Weast, Ed., *Handbook of Chemistry and Physics*, 70th Ed. Boca Raton, FL: CRC, 1990, pp. F197–F200.
[43] ——, *Handbook of Chemistry and Physics*, 70th Ed. Boca Raton, FL: CRC, 1990, pp. F206–F209.
[44] B. Chapman, *Glow Discharge Processes*. New York: Wiley-Interscience, 1980, p. 16.
[45] K. Tsujimoto, T. Kumihashi, N. Kofuji, and S. Tachi, "High-rate-gas-flow microwave plasma etching of silicon," in *Tech. Dig. 1992 VLSI Symp.*, Seattle, pp. 46–47.
[46] K. Tsujimoto, T. Kumihashi, and S. Tachi, "Novel short-gas-residence-time electron cyclotron resonance plasma etching," *Appl. Phys. Lett.*, vol. 63, no. 14, pp. 1915–1917, 1993.
[47] B. N. Chapman and V. J. Minkiewicz, "Flow rate effects in plasma etching," *J. Vac. Sci. Technol.*, vol. 15, no. 2, pp. 329–332, 1978.
[48] B. N. Chapman, T. A. Hansen, and V. J. Minkiewicz, "The implication of flow-rate dependencies in plasma etching," *J. Appl. Phys.*, vol. 51, no. 7, pp. 3608–3613, 1980.
[49] K. Ino and T. Ohmi, "Modeling and analysis of RF plasma using electrical equivalent circuit," in *Ext. Abstr. Int. Conf. Solid State Devices and Materials*, Osaka, 1995, pp. 644–646.
[50] K. Köhler, D. E. Horne, and J. W. Coburn, "Frequency dependence of ion bombardment of grounded surfaces in rf argon glow discharge in a planar system," *J. Appl. Phys.*, vol. 58, no. 9, pp. 3350–3355, 1985.
[51] V. A. Godyak, R. B. Piejak, and B. M. Alexandrovich, "Electrical characteristics of parallel-plate RF discharge in argon," *IEEE Trans. Plasma Science*, vol. 19, no. 4, pp. 660–676, 1991.

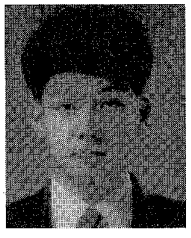

Kazuhide Ino was born in Saitama, Japan, on March 31, 1970. He received the B.S. and M.S. degrees in electronic engineering from Tohoku University, Sendai, Japan, in 1992 and 1995, respectively.

He is currently working on high performance plasma process and ultra-low-resistance contact metallization toward the Ph.D. degree at Tohoku University.

Mr. Ino is a member of the Institute of Electronics, Information and Communication Engineers of Japan.

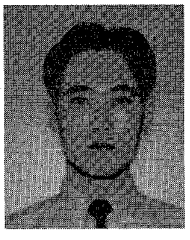

Iwao Natori was born in Yamanashi, Japan, on September 11, 1962. He received the B.S. degree in environmental engineering from Yamanashi University in 1986.

In 1986, he joined Hitachi Tokyo Electronics Co. Ltd., where he worked in controlling of process in LSI manufacturing. From 1990 to 1993, he was a Visiting Researcher, Faculty of Engineering, Tohoku University, where he carried out research on high performance reactive ion etching and related microfabrication technology. At present, he is carrying out the development on ion etching process.

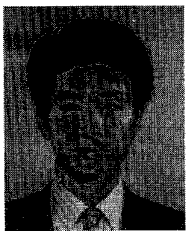

Akihiro Ichikawa was born in Chiba, Japan, on January 29, 1964. He received the B.S. and M.S. degrees in environmental engineering from Kyushu Institute of Technology in 1987 and 1989, respectively.

In 1989, he joined Nippon Sanso Corp., where he worked in gas purification. From 1992 to 1995, he was a Visiting Researcher, Faculty of Engineering, Tohoku University, where he carried out research on high performance reactive ion etching process and related microfabrication technology. He is now studying CVD process using ultra pure gases which contain lower concentration of metals and moisture.

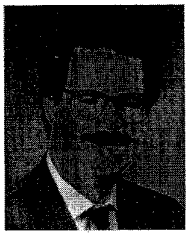

Raymond N. Vrtis was born on January 18, 1963. He received the B.S. degree in chemistry from the University of Illinois in 1985, and the Ph.D. degree in organometallic chemistry from the Massachusetts Institute of Technology in 1989. He was also a postdoctoral associate in organometallic chemistry at the University of California, Berkeley, for one and a half years.

He has authored nine scientific articles and has four patents. He has worked at Schumacher since 1991, spending one of those years in Japan working with Professor Tadahiro Ohmi at Tohoku University under the auspices of Air Products and Chemicals.

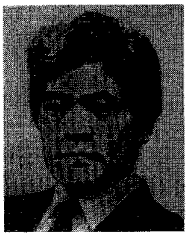

Tadahiro Ohmi (M'81) was born in Tokyo, Japan on January 10, 1939. He received the B.S., M.S., and Ph.D. degrees in electrical engineering from Tokyo Institute of Technology, Tokyo, in 1961, 1963 and 1966, respectively.

Prior to 1972, he served as a Research Associate, Department of Electronics, Tokyo Institute of Technology, where he worked on Gunn diodes such as velocity overshoot phenomena; multi-valley diffusion and frequency limitation of negative differential mobility due to an electron transfer in the multi-valleys; high-field transport in semiconductor such as unified theory of space-charge dynamics in negative differential mobility materials; Bloch-oscillation-induced negative mobility and Bloch oscillators; and dynamics in injection layers. He is presently a Professor, Department of Electronics, Faculty of Engineering, Tohoku University. He is engaged in research on high-performance ULSI such as ultra-high-speed USLI; current overshoot transistor LSI; HBT LSI and SOI on metal substrate; and base store image sensor(BASIS) and high-speed flat-panel display. He is also reasearching advanced semiconductor process technologies, i.e., ultra-clean technologies such as high-quality oxidation; high-quality metallization due to low kinetic energy particle bombardment; very-low-temperature Si epitaxy particle bombardment; crystallinity control film growth technologies from single-crystal; grain-size-controlled polysilicon and amorphous due to low kinetic energy particle bombardment; *in situ* wafer surface cleaning technologies due to low kinetic energy particle bombardment; highly selective CVD; highly selective RIE; high-quality ion implantation with low-temperature annealing capability etc., based on the new concept supported by newly developed ultra-clean gas supply system; ultra-high vacuum-compatible reaction chamber with self-cleaning function; ultra-clean wafer surface cleaning technology etc.

Dr. Ohmi's research activities are as follows: 512 original papers and 522 patent applications. He received the Ichimura Award in 1979, the Teshima Award in 1987, the Inoue Harushige Award in 1989, the Ichimura Prizes in Industry-Meritorious Achievement Prize in 1990, and the Okochi Memorial Technology Prize in 1991. He serves as the President, Institute of Basic Semiconductor Technology-Development (Ultra Clean Society). Dr. Ohmi is a member of the Institute of Electronics, Information and Communication Engineers of Japan, the Institute of Electrical Engineers of Japan, the Japan Society of Applied Physics, and the ECS.